DYNAMIC LIGHT SCATTERING FROM POLYDISPERSE SUSPENSIONS OF THIN ELLIPSOIDAL SHELLS OF REVOLUTION WITH SUBMICRON DIAMETERS

SATORU FUJIME, MICHIHO TAKASAKI-OHSITA, AND SHIGEAKI MIYAMOTO
Mitsubishi-Kasei Institute of Life Sciences, Machida, Tokyo 194, Japan

ABSTRACT: Osmotic swelling of membrane vesicles has been studied in combination with dynamic light scattering, to obtain information about the elastic properties of biomembranes. In such studies, there arise some technical problems specific to dynamic light scattering, which include the effects on the light-scattering results of the size distribution and nonsphericity of the vesicles with submicron sizes. Even for highly monodisperse suspensions of spherical vesicles (σ/d_n = [(the mean of d^2)$/d_n^2 - 1]^{1/2} = 0.1$; d_n being the number-average diameter of vesicles), the average diameter d obtained from dynamic light scattering is shown to be strongly dependent on d_nK, where K is the length of the scattering vector. This is solely due to the shell structure of the vesicles. For ellipsoidal vesicles, another complication appears which is due to the rotational motion of ellipsoids.

INTRODUCTION

The elastic modulus of the membrane vesicles was recently measured by an osmotic swelling method (Li et al., 1986; Sun et al., 1986). The protocol of this method is as follows: Vesicles (spherical in shape) with an initial diameter d_o are prepared in an aqueous solution containing C_o (mol/l) of solute. A dilution buffer is then added to the sample in the scattering cell to reduce the final external concentration of the solute to C_e. Assume that the vesicle is permeable to water but not to the solute. Then, water flows into the vesicle, and the vesicle expands until the final internal concentration C_i of solute is reached with the final diameter d_f, where the osmotic pressure difference, $P_1 - P_2$, across the vesicle wall just balances against the elastic force produced by the expansion. Van't Hoff's law gives $P_1 - P_2 = K_o(C_i - C_e)$, where K_o is the osmotic coefficient. On the other hand, the stress, T_s, which induces the change in the membrane area, $\Delta A = (d_f^2 - d_o^2)/d_o^2$, can be given by $T_s = (d_f/4)(P_1 - P_2)$. The elastic modulus, M (dyn/cm), is defined by $T_s = M\Delta A$. By noting $C_i = (d_o/d_f)^3C_o$, the following relation is established (Li et al., 1986; Sun et al., 1986; Miyamoto et al., 1988);

$$d_o/d_f = \frac{d_o^2 d_f K_o}{4(d_o + d_f)}(1/M)[(d_o - d_f)^3C_o - C_e] \qquad (1)$$

The dynamic light-scattering method can be used to obtain the exact value of the average diameter of the membrane vesicles in the solution. General background information about the dynamic light-scattering method is found in standard textbooks (Chu, 1974; Berne and Pecora, 1975). The intensity correlation function, $G^2(\tau)$, of the scattered light is related to the normalized field correlation function, $g^1(\tau)$, of the scattered light by

$$G^2(\tau) = B[1 + \beta|g^1(\tau)|^2] \qquad (2)$$

where B is the baseline and β is a constant. For a polydisperse system, $g^1(\tau)$ is generally expressed as

$$g^1(\tau) = \int_0^\infty G(\Gamma)\exp(-\Gamma\tau)\,d\Gamma \text{ with } \int_0^\infty G(\Gamma)\,d\Gamma = 1, \qquad (3)$$

where $G(\Gamma)$ is the distribution function of the decay rate Γ of $g^1(\tau)$. To obtain the average decay rate Γ of $g^1(\tau)$, the cumulant expansion method is routinely adopted (Koppel, 1972):

$$g^1(\tau) = \exp[-\bar{\Gamma}\tau + (\mu_2/2!)\tau^2 - (\mu_3/3!)\tau^3], \qquad (4)$$

where $\bar{\Gamma} = \int \Gamma G(\Gamma)\,d\Gamma$ and $\mu_n = \int(\Gamma - \bar{\Gamma})^n G(\Gamma)\,d\Gamma$. $(\mu_2/\bar{\Gamma}^2)$ is a measure of the dispersion in $G(\Gamma)$. The average diffusion coefficient, D, and the diameter, d, of the membrane vesicle can be obtained, respectively, by

$$\bar{\Gamma} = DK^2 \quad \text{and} \quad D = k_BT/(3\pi\eta d), \qquad (5)$$

where $K = (4\pi n_s/\lambda_o)\sin(\theta/2)$ is the length of the scattering vector $\mathbf{K}$ (n_s: the refractive index of the solvent, λ_o: vacuum wavelength of the incident light, and θ: the scattering angle), k_B is the Boltzmann constant, T is the absolute temperature, and η is the solvent viscosity.

The osmotic swelling method in combination with the dynamic light scattering method seems to be very powerful, especially for vesicles with submicron sizes, such as brush border membrane vesicles, secretory granules and synaptic vesicles in the presynaptic axon. In connection with our own swelling experiments on brush border membrane vesicles in an accompanying paper (Miyamoto et al.,

1988), we describe some technical problems specific to dynamic light scattering from suspensions of ellipsoidal shells of revolution as well as spherical shells. The problems include the effects of the size distribution and of nonsphericity of the scatterers on the light-scattering results. They have not been discussed explicity by previous researchers. Our results show that the D value of spherical vesicles strongly depends on K, and that the D value of ellipsoidal vesicles with the axial ratio as small as two shows quite different dependence upon K from that of spherical vesicles. To discuss them, we list below the relevant formulas for later convenience.

For an ellipsoidal shell of revolution, $x^2/b^2 + y^2/b^2 + z^2/a^2 = 1$, with thickness $t_o \ll \lambda_o$, the amplitude of the scattered light at time t can be written as (Fujime and Kubota, 1985)

$$e(t) = \exp[i\mathbf{K} \cdot \mathbf{R}(t)]a(K, \xi, t) \quad (6)$$

$$a(K, \xi, t) = j_0(Z) = (\sin Z)/Z \quad (7)$$

$$Z = Kb[1 - (1 - p^{-2})\xi^2]^{1/2} = Kb(1 - q\xi^2)^{1/2} \quad (8a)$$

$$q = 1 - p^{-2}, \quad (8b)$$

where $\mathbf{R}(t)$ is the position vector of, ξ is the cosine of the instantaneous angle between the vector $\mathbf{K}$ and the z-axis of, the ellipsoidal shell, and $p = b/a$ is the axial ratio; $p > 1$ (oblate), $p = 1$ (spherical) and $0 < p < 1$ (prolate). The unnormalized field correlation function is given by

$$G^1(\tau) = G_D(\tau) \sum_n \sum_m (2m + 1) \cdot [U \exp(-\Theta\Lambda\tau)U^{-1}]_{n,m} a_n(Kb) a_m(Kb) \quad (9)$$

$$a_n(Kb) = \int_0^1 j_0(Z)P_n(\xi)\, d\xi \quad \text{(for even } n\text{)}$$
$$= 0 \quad \text{(for odd } n\text{)}, \quad (10)$$

where $G_D(\tau) = \exp(-[D_0 - (1/3)(D_3 - D_1)]K^2\tau)$, $\tau = |t - t'|$, D_3 and D_1 are, respectively, the translational diffusion coefficients parallel and perpendicular to the z-axis of the ellipsoidal shell ($D_0 = (2D_1 + D_3)/3$ is the overall diffusion coefficient), Θ is the rotational diffusion coefficient around the $x(y)$ axis of the ellipsoidal shell, $P_n(\xi)$ is the Legendre polynomial of the order n, and the explicit forms of the matrices U and Λ are found elsewhere (Maeda and Fujime, 1984; these matrices describe the effect of anisotropy, $D_1 \neq D_3$). The static scattering function is given by

$$P(Kb) = G^1(0) = \sum_n (2n + 1)a_n(Kb)^2 = \int_0^1 j_0(Z)^2\, d\xi, \quad (11)$$

where use was made of $UU^{-1} = E$ (the unit matrix). The last form of $P(Kb)$ in Eq. 11 has been derived by Norisuye and Yu (1977). From time derivative of Eq. 9, the first cumulant $\bar{\Gamma}$ of $G^1(\tau)$ is given by

$$\bar{\Gamma}/K^2 = D_0 + b^2\Theta g_1(Kb) + (D_3 - D_1)[g_2(Kb) - 1/3] \quad (12)$$

$$g_1(Kb) = (Kb)^{-2} \sum_n n(n + 1)(2n + 1)a_n(Kb)^2/P(Kb) \quad (13)$$

$$g_2(Kb) = \sum_n (2n + 1)a_n(Kb)[L_0(n)a_n(Kb) + L_2(n - 2)a_{n-2}(Kb) + L_1(n + 2)a_{n+2}(Kb)]/P(Kb). \quad (14)$$

The explicit forms of $L_i(n)$ are found elsewhere. The details of the derivation of the above equations, and numerical results for $p \gg 1$ and $0 < p \ll 1$ are found in Fujime and Kubota (1985).

EFFECT OF POLYDISPERSITY

Spherical Shells ($p = 1$)

Let us denote the size distribution by $N(z)$ where $z = d/d_n$ (d_n being the number-average diameter of the vesicles). The light-scattering average is the so-called z-average, which is denoted by $\langle \ldots \rangle$. Although the size of the spherical shells of our interest is very large, the scattering function for a spherical shell, with wall thickness $t_o \ll \lambda_o$, is precisely given by Eq. 11, $P(x) = \sin^2(x)/x^2$ with $x = Kb = Kd/2$ (i.e., no violation of the so-called Rayleigh-Debye condition). Then, we have

$$\langle g^1(\tau) \rangle = \int P(x) \exp[-D(d)K^2\tau]z^4N(z)\, dz / \int P(x)z^4N(z)\, dz, \quad (15)$$

where $D(d)$ is the diffusion coefficient of a sphere with diameter d. Eq. 15 is a d-space version of Eq. 3. The time derivatives of Eq. 15 at $\tau = 0$ give

$$\langle D^i \rangle = \int D(d)^i(x)z^4N(z)\, dz / \int P(x)z^4N(z)\, dz. \quad (16)$$

To carry out integration of Eq. 16 explicitly, we assume the Schulz-Zimm distribution function without the normalization factor: $N(z) = z^m \exp[-(m + 1)z]$, where m is the measure of the sharpness of the distribution; $\sigma/d_n = [(\text{the mean of } d^2)/d_n^2 - 1]^{1/2} = (m + 1)^{-1/2}$. By use of the following integral formula for $(a, \alpha) > 0$ (Moriguchi et al., 1959)

$$\int_0^\infty \exp(-az)z^{\alpha-1} \cos(bz)\, dz = \frac{\Gamma(\alpha)}{(a^2 + b^2)^{\alpha/2}} \cos[\alpha \tan^{-1}(b/a)] \quad (17)$$

and $\sin^2(x) = [1 - \cos(2x_n z)]/2$ where $x_n = Kd_n/2$, we easily have

$$\frac{\langle D^i \rangle}{D(d_n)^i} = \frac{2(m + 1)^i(m + 2 - i)!}{(m + 4)!} \times \frac{1 - \cos[(m + 3 - i)\tan^{-1}(y)]/(1 + y^2)^{(m+3-i)/2}}{y^2\langle P(x) \rangle} \quad (18)$$

$$(\mu_2/\bar{\Gamma}^2) = \langle D^2 \rangle / \langle D \rangle^2 - 1, \quad (19)$$

where $y = 2x_n/(m + 1)$ and $D(d_n)$ is the diffusion

coefficient of the particle with diameter d_n. For $i = 0$, Eq. 18 gives $\langle P(x)\rangle$. A very similar expression to our $\langle P(x)\rangle$ has been derived from a slightly different model from ours (Aragon and Pecora, 1976). At $K = 0$, we have $\langle D\rangle^\circ = [(m+1)/(m+4)]D(d_n)$, $\langle D^2\rangle^\circ = [(m+1)^2/(m+3)/(m+4)]D(d_n)^2$, and $(\mu_2/\bar{\Gamma}^2)^\circ = (m+3)^{-1}$.

Ellipsoidal Shells of Revolution ($p \neq 1$)

From Eqs. 8 and 11, the scattering function for $p \neq 1$ can be written as

$$P(x) = \int_0^1 \frac{\sin^2 [x(1 - q\xi^2)^{1/2}]}{x^2(1 - q\xi^2)}\, d\xi. \qquad (20)$$

By replacing $y = 2x_n/(m+1)$ in Eq. 18 with $v = y(1 - q\xi^2)^{1/2}$, and integrating over ξ, we immediately have the theoretical expressions of $\langle P(x)\rangle$, $\langle D\rangle$ and $(\mu_2/\bar{\Gamma}^2)$ for the ellipsoidal shell of revolution with D(ellipsoid with the axial ratio p) = D(sphere) $\times$ $pG_0(p)$, where $G_0(p)$ is the shape factor depending only on p (Perrin, 1934). (As shown below, the rotational motion of the scatterers with slight nonsphericity does not have an appreciable effect on the result.) Numerical integration over ξ is easily carried out by use of any desk-top computer because of the well-behaved integrand.

NUMERICAL RESULTS

The numerical results are graphically shown; $x_n^2\langle P(x)\rangle$ in Fig. 1, $\langle D\rangle$ in Fig. 2 *a*, and $(\mu_2/\bar{\Gamma}^2)$ in Fig. 2 *b*. For slight nonsphericity ($p = 1.2$, oblate; and $p^{-1} = 1.2$, prolate), these quantities behave very similarly to those for a spherical shell ($p = 1$). Note that we put $b = d/2$ and $a = b/1.2$ ($p = 1.2$), and $a = 1.2b$ ($p^{-1} = 1.2$); the volumes $V(p) = (4/3)\pi b^3/p$ of the shells were in the order of $V(1.2^{-1}) > V(1) > V(1.2)$. This situation appeared, for example, in the peak positions of the curves in Figs. 1 and 2.

As a function of x_n, the modified intensity $x_n^2\langle P(x)\rangle$ of a spherical shell changes like $\sin^2(x_n)$ for $m = \infty$ (monodisperse). With the decreasing m value (decreasing monodispersity), the modified intensity shows a damped oscillation (Fig. 1). The modified intensity of an ellipsoidal shells also shows a damped oscillation even for $m = \infty$. From the static intensity alone, it is therefore very difficult to conclude that the sample is the suspension of monodisperse ellipsoidal shells, of polydisperse spherical shells, or of polydisperse ellipsoidal shells, as has been reviewed by Yu (1983).

One of our notable predictions is the K^2-dependence of $\langle D\rangle$ (Fig. 2 *a*). Even for a very sharp size-distribution, $m = 100$ (or relative dispersion of $\sigma/d_n = 0.1$), $\langle D\rangle$ depends largely on x_n^2 (or K^2). In Fig. 2, the vertical bars show the x_n^2 values for the indicated diameters (in nanometers) of the vesicle at the scattering angle of 90°. To simulate the experimental result of $\langle D\rangle$, we computed the field correlation functions according to Eq. 15, by assuming $\tau = m\Delta\tau (m = 1, 2, \ldots, 128)$, $D(d_n)K^2(128\Delta\tau) = 2$, $m = 10$, $d_n = 330$ nm and $p = 1$. The $G^2(\tau)$s were

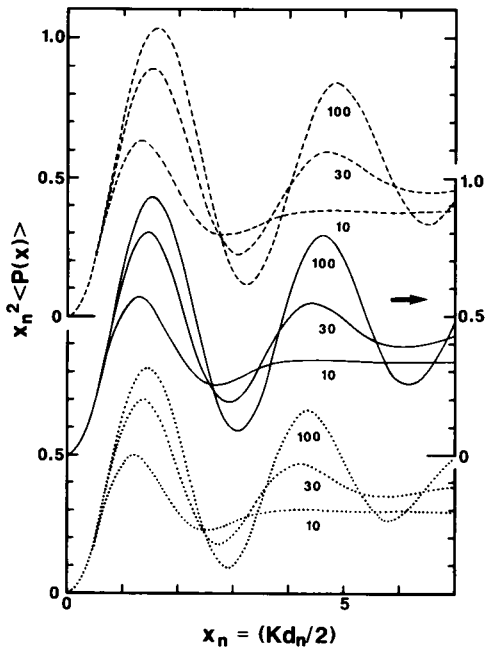

FIGURE 1 The $x_n^2\langle P(x)\rangle$ vs. x_n relationships for suspensions of ellipsoidal shells of revolution. The dashed lines are for $p = b/a = 1.2$ (oblate ellipsoidal), the solid lines for $p = 1$ (spherical), and the dotted lines for $p^{-1} = 1.2$ (prolate ellipsoidal); $x_n = Kd_n/2 = Kb_n$. The values of the distribution parameter, m, are indicated on the figure.

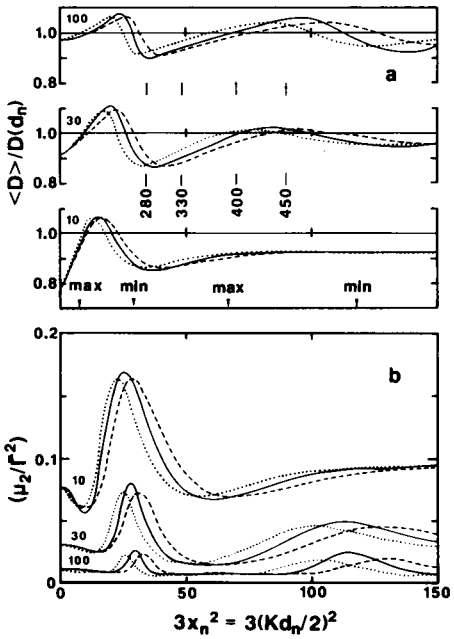

FIGURE 2 The $\langle D\rangle$ vs. x_n^2 (in *a*) and $(\mu_2/\bar{\Gamma}^2)$ vs. x_n^2 (in *b*) relationships for suspensions of ellipsoidal shells of revolution. The dashed lines are for $p = 1.2$ (oblate ellipsoidal), the solid lines for $p = 1$ (spherical), and the dotted lines for $p^{-1} = 1.2$ (prolate ellipsoidal); $x_n = Kd_n/2 = Kb_n$. The values of the distribution parameter, m, are indicated on the figure. The vertical bar with number xxx indicates the position of the $3x_n^2$ value for d = xxx nm and the scattering angle of 90°. Arrows indicate the positions of the minima and maxima of $\sin^2(x_n)$.

constructed by a formula, $G^2(\tau) = B + [B|g^1(\tau)|^2 + B^{1/2}n(\tau)]$, where $|n(\tau| \leq 1$ provided a random noise, and $\beta = 1$ was assumed (cf., Eq. 2). For $B = 10^5$ (relative noise level of 0.3%) and successively generated random noise $n(\tau)$, ten $G^2(\tau)$s at each K^2 were analyzed by use of Eq. 4. At this noise level, the standard deviation (SD) for these ten successive results were $(0.002 - 0.004)\langle D\rangle$ in $\langle D\rangle$ and 0.015 – 0.030 in $(\mu_2/\bar{\Gamma}^2)$. The average values of $\langle D\rangle$ and $(\mu_2/\bar{\Gamma}^2)$ were compared in Fig. 3 with the corresponding curves, Eqs. 18 and 19. Agreement was perfect in $\langle D\rangle$ values, but not very good in $(\mu_2/\bar{\Gamma}^2)$, especially in the second-order analysis.

If such characteristic behavior of $\langle D\rangle$ against K^2 as shown in Figs. 2 and 3 is observed for a given sample, the shape of vesicles will be very close to a sphere. If the K^2 value at the measurement of $G^2(\tau)$s is in a range of a positive (negative) slope of $\langle D\rangle$ against x_n^2, the expansion of the vesicle by osmotic swelling is under/over-estimated, because the expansion shifts the x_n^2 value for a given K^2 right wards on the abscissa of Figs. 2 a and 3 a. Even when the light-scattering measurements were carried out perfectly, the error due to this source would be the most serious in determining the $(d_o/d_f)^3$ and hence the M values in Eq. 1. Carefull examinations of the dependence on K^2 of the $\langle D\rangle$ values around the point of the measurement are very important.

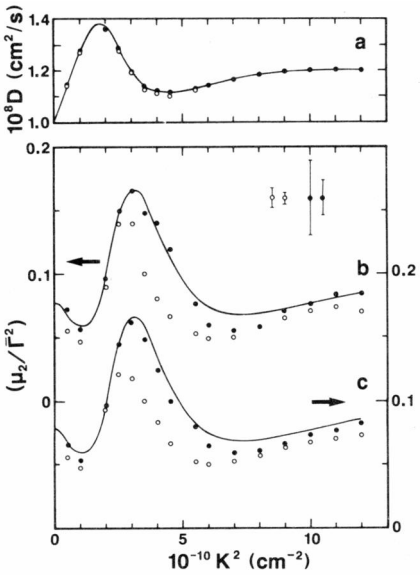

FIGURE 3 The results of the cumulant expansion of theoretically constructed correlation functions for a polydisperse suspension of spherical shells (d_n = 330 nm and m = 10). Filled circles are from the third-order expansion, and open circles from the second-order expansion. The solid lines are the theoretical curves shown in Fig. 2. (*a*) The $\langle D\rangle$ vs. K^2 relationships, where $10^8D(d_n) = 1.3$ cm^2/s. Open symbols overlapped with filled ones are not shown. Error sizes are within the radius of symbols for 0.3 and 0.03% noise levels. (*b*) The $(\mu_2/\bar{\Gamma}^2)$ vs. K^2 relationships for the 0.3% noise levels. Error bars are shown at the corner. (*c*) The $(\mu_2/\bar{\Gamma}^2)$ vs. K^2 relationships at the 0.03% noise level. Error sizes are within the size of symbols. For details, see text.

Effect of Rotational Motion of Ellipsoidal Shells

For the axial ratio $p = 1$ (or $q = 0$), $j_0(Z) = j_0(Kb)$ in Eq. 7 is independent of ξ, so that Eq. 10 gives $a_n(Kb) = 0$ for $n \geq 1$; namely, $g_1(Kb) = 0$ and $g_2(Kb) = 1/3$, and no effect of the rotational motion on $\langle D\rangle$ and $(\mu_2/\bar{\Gamma}^2)$. For $p \neq 1$, on the other hand, $a_n(Kb)$s for even n (≥ 2) are not necessarily zero for submicron sizes of the scatterer. Fig. 4 shows $a_n(Kb)s$ for slightly oblate (p = 1.2) and $a_n(Ka)$s for slightly prolate (p^{-1} = 1.2) ellipsoidal shells of revolution. (For $p < 1$, we put $Z = Ka[p^2 + (1 - p^2)\xi^2]^{1/2}$ instead of Eq. 8a.) Qualitatively speaking, a_0 comes from sphericity of, and a_2 from the first order nonsphericity of, the ellipsoidal shell of revolution. It should be noted that at the zero points of a_0, $|a_2|$ is near one of its maxima. Thus, both $g_1(Kb)$ in Eq. 13 and $g_2(Kb)$ in Eq. 14 have large values at these points; $g_1(Kb) \sim 6/(Kb)^2 = 0.54$ and $g_2(Kb) \sim L_0(2) = 0.52$ at the first zero point of $a_0(Kb)$. Then, the $\langle D\rangle$ values of the ellipsoidal shells of revolution shown by dashed and dotted lines in Fig. 2 are substantially modified by the contribution to $\bar{\Gamma}/K^2$ from the rotational motion of the ellipsoidal shell, if the sample is highly monodisperse ($m \geq 100$). Numerical examinations, however, showed that the effect is negligibly small for $m \leq 30$.

Fig. 5 shows $a_n(Kb)$s for $p = 2$ and $a_n(Ka)$s for $p^{-1} = 2$. Except for the relative sizes of $a_n(Kb)$s [and $a_n(Ka)$s], general behaviors of these curves are very similar to those in Fig. 4. In these cases, however, the second and third terms in Eq. 12 have substantial contributions to $\langle\bar{\Gamma}/K^2\rangle$ even for $m \leq 30$. To examine this situation, we assumed Perrin's formulas for the diffusion coefficients, D_0, D_1, D_3, and Θ, of an ellipsoid of revolution (Perrin, 1934).

Fig. 6 shows the $\langle\bar{\Gamma}/K^2\rangle$ vs. K^2 relationships for the ellipsoidal shells of revolution with $p > 1$ (left panel) and $p^{-1} > 1$ (right panel). The contribution from the second and third terms in Eq. 12 amounts to $\langle b^2\Theta g_1(Kb)\rangle + \langle(D_3 - D_1)[g_2(Kb) - 1/3]\rangle = 0.228 - 0.034 = 0.194$ in

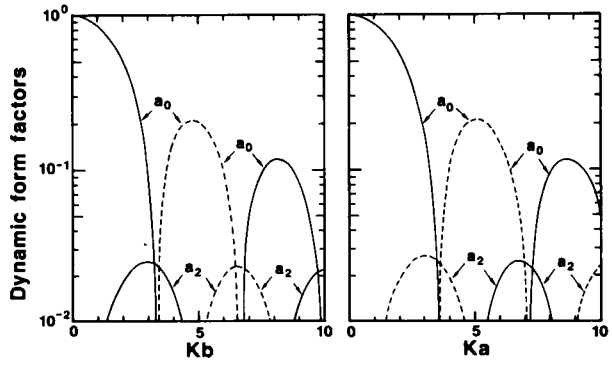

FIGURE 4 Graphic representation of the dynamic form factors. Left panel: $a_n(Kb)$ for a slightly oblate ellipsoidal shell of revolution (p = 1.2), and right panel: $a_n(Ka)$ for a slightly prolate ellipsoidal shell of revolution (p^{-1} = 1.2). The dashed parts have the negative sign.

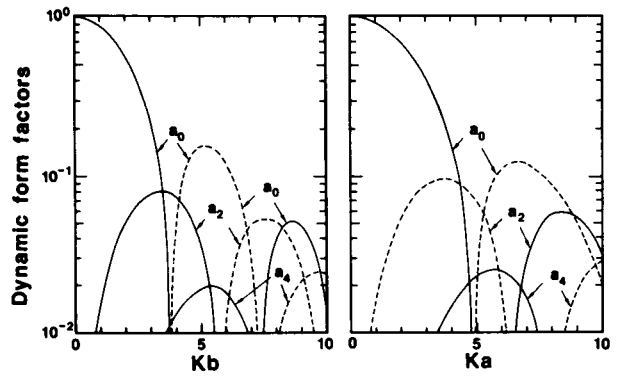

FIGURE 5 Graphic representation of the dynamic form factors. Left panel: $a_n(Kb)$ for $p = 2$, and right panel: $a_n(Ka)$ for $p^{-1} = 2$ ($p = 0.5$). The dashed parts have the negative sign.

units of $D_0(b_n)$, for example, at $3(Kb_n)^2 = 32$ and $p = 2$. On the abscissa, 49 corresponds to the scattering angle of 90° for $2b_n$ (and $2a_n$) = 330 nm.

In the above numerical simulation, we assumed the polydispersity parameter of $m = 10$. This value of m is not too bad for biological membrane vesicles, because the number of vesicles with the sizes smaller than $0.5d_n$ and larger than $2d_n$ is only 3% of the total [for profiles of $N(z)$ for some m values, see Fig. 7 given below]. It should be noted that the effect of the rotational motion on the apparent diffusion coefficient is very large even for the axial ratio as small as two ($p = 2$ and 0.5).

Decay-Rate Distribution

Here we consider again a polydisperse suspension of spherical shells. Let us define $F(z) = [\sin^2(x_n z)/x_n^2]z^2N(z)/\int P(x)z^4N(z)\,dz$ (see Eq. 15). Since $D(d) = D(d_n)/z$ or $\Gamma(z) = D(d_n)K^2/z$, we have $d\Gamma = -dz/z^2$. Then, we have

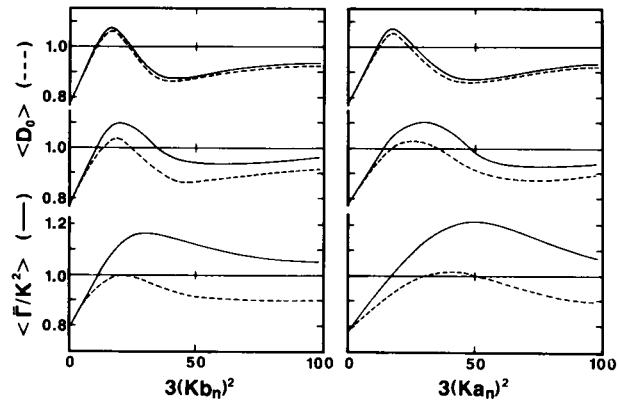

FIGURE 6 The $\langle\bar{\Gamma}/K^2\rangle$ and $\langle D_0\rangle$ vs. K^2 relationships in units of D_n. The solid lines show $\langle\bar{\Gamma}/K^2\rangle$ and the dotted lines show $\langle D_0\rangle$. Left panel: $2b_n$ = 330 nm, $D_n = (k_BT/6\pi\eta b_n)pG_0(p)$, $m = 10$, and $p = 1.2$, 1.5, and 2.0 from top to bottom. The right panel: $2a_n = 330$ nm, $D_n = (k_BT/6\pi\eta a_n)G_0(p)$, $m = 10$, and $p^{-1} = 1.2$, 1.5, and 2.0 from top to bottom. $G_0(p)$ denotes the shape factor (Perrin, 1934). On the abscissa, 49 corresponds to the scattering angle of 90°.

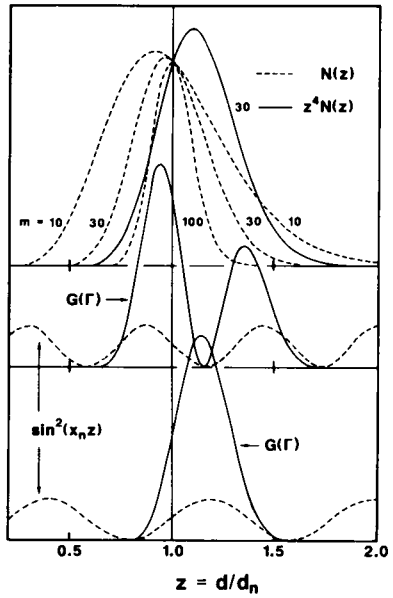

FIGURE 7 The simulated results of G(Γ) for a suspension of spherical shells. The upper part shows $N(z)$s for $m = 100$, 30, and 10 by the dashed lines, and $z^4N(z)$ for $m = 30$ by the solid line, where $N(1)$ is normalized to unity. The middle part shows $\sin^2(x_n z)$ for $d_n = 330$ nm and the scattering angle of 150° by the dashed line, and G(Γ) for $m = 30$ by the solid line. The lower part shows the same quantities as those in the middle part, but for the scattering angle of 90°. Very minor side-peaks in G(Γ)s were ignored.

G(Γ) defined in Eq. 3 as

$$G(\Gamma)d\Gamma \propto F(z)\,dz \propto \sin^2(x_n z)z^4N(z)\,d\Gamma. \qquad (21)$$

For a given m value (a given size distribution), the profile of G(Γ) has a single peak for the x_n value where one of peaks of $\sin^2(x_n z)$ comes close to the peak of $z^4N(z)$, whereas double peaks for the x_n values where one of zeros of $\sin^2(x_n z)$ comes close to the peak of $z^4N(z)$, namely, the profile of G(Γ) strongly depends on the x_n value. These situations are illustrated with two examples in Fig. 7. Needless to say, the moments of G(Γ) in Eq. 16 give the same results from Eq. 3 in spite of apparent differences in the profiles of G(Γ) from angle to angle.

The factor $\sin^2(x_n z)$ works as a broad "notch filter" to 'eliminate' particles with sizes around d which satisfies $x_n z = \nu\pi$ (ν being positive integers). Note the points of the minima and maxima of $\sin^2(x_n z)$ for $z = 1$, which are indicated by arrows on the lower frame of Fig. 2 *a*. For the axial ratios slightly different from unity (slightly elllipsoidal shells), the minimum values of the modified intensity $(x_n z)^2P(x_n z)$ of Eq. 20 (which reduces to $\sin^2(x_n z)$ for $p = 1$ or $q = 0$) are small but not zero; for $p = 1.2$ ($p^{-1} = 1.2$), for example, the first maximum, 1.11 (0.87); the second minimum, 0.032 (0.028); the second maximum, 1.05 (0.82); the third minimum, 0.12 (0.10); ... However, $(x_n z)^2P(x_n z)$ still works as the notch filter in the above sense. It should be noted that the points indicated by 'min'

('max') in Fig. 2 *a* correspond to the peak (minimum) positions of $(\mu_2/\bar{\Gamma}^2)$ in Fig. 2 *b*. This clear correspondence is solely due to the K-dependent profile of $G(\Gamma)$ as depicted in Fig. 7.

Eq. 1 is rewritten approximately as $M \doteqdot (K_o/8)d_f[C_o - C_e]/\epsilon$, where $\epsilon = (d_f - d_o)/d_o$. Since M is the material constant, it hardly depends on the vesicle size larger than a certain value (out of the curvature-limited sizes). Then, for a given C_e value, the larger the vesicle diameter is, the larger the expansion rate (ϵ) is. Because of the factor $\sin^2(x_n z)$ (see $G(\Gamma)$s in Fig. 7), the observed ϵ values at different scattering angles have slightly different meanings from each other, even when they are equal in magnitude.

Brush Border Membrane Vesicles

As an experimental example, Fig. 8 shows the $K^2P(K)$ vs. K^2 and $\bar{\Gamma}/K^2$ vs. K^2 relationships for a suspension of the brush border membrane vesicles prepared from rat small intestine. The experimental details are found in the accompanying paper (Miyamoto et al., 1988). The peak position and peak-to-minimum ratio in the $K^2P(K)$ vs. K^2 relationship suggest $\langle a \rangle \sim 200$ nm and $m \sim 15$ for $p = 0.5$, $\langle d/2 \rangle \sim 140$ nm and $m \sim 10$ for $p = 1$, and $\langle b \rangle \sim 160$ nm and $m \sim 15$ for $p = 2$. Since only one peak and one valley in $K^2P(K)$ could be observed in the accessible range of K, any definite conclusion could not be extracted. Among these, however, the $p = 0.5$ case is compatible with the relative positions of the peak and minimum in $K^2P(K)$. The profile of $\bar{\Gamma}/K^2$ against K^2 does not show such a feature characteristic of spherical and/or slightly ellipsoidal shells as shown in Fig. 2, but it suggests $p \sim 0.5$ (and not $p \sim 2$; cf., Fig. 6).

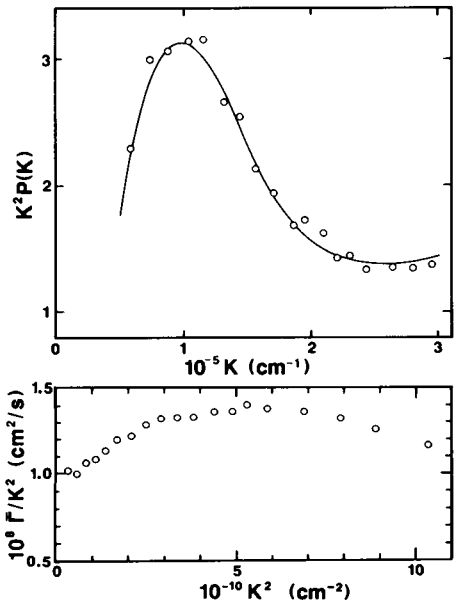

FIGURE 8 An experimental example for a suspension of brush border membrane vesicles prepared for rat small intestine (Miyamoto et al., 1988). $K^2P(K)$ is in an arbitrary scale. The solid line is for $a_n = 200$ nm, $m = 15$ and $p = 0.5$.

The limiting value of $\bar{\Gamma}/K^2 = 1.0 \times 10^{-8}$ cm^2/s at $K^2 = 0$ gives $\langle 1/a \rangle^{-1} \sim 320$ nm for $p = 0.5$, $\langle 2/d \rangle^{-1} \sim 210$ nm for $p = 1$, and $\langle 1/b \rangle^{-1} \sim 250$ nm for $p = 0.5$. These average sizes of vesicles from the $\bar{\Gamma}/K^2$ are 1.5 times larger than the corresponding ones from the static scattering intensity. This came from, at least, two sources. The first source is the different weights in the average over size distribution; $\langle D \rangle^o/D(d_n) = \int z^3 N(z)\, dz/M_r$ at $K^2 = 0$ and $x_n^2\langle P(x) \rangle = \int \sin^2(x_n z) z^2 N(z)\, dz/N_r$ (for sphere, for example) with the normalization constant $N_r = \int z^4 N(z)\, dz$. Since the maximum of $z^2N(z)$ appears at $z = (m + 2)/(m + 1)$, the $\langle x \rangle$ value which satisfies $[(m + 2)/(m + 1)]\langle x \rangle = \pi/2$ gives the largest overlap between $\sin^2(\langle x \rangle z)$ and $z^2N(z)$, and hence the first maximum of $x_n^2\langle P(x) \rangle$. Then, we have $\langle d \rangle = [(m + 1)/(m + 2)]d_n$. (Note the shift of the first peak with m in Fig. 1.) From the relation $\langle D \rangle^o = [(m + 1)/(m + 4)]D(d_n)$ given above, on the other hand, we immediately have $\langle 1/d \rangle^{-1} = [(m + 4)/(m + 1)]d_n$. From these simple considerations, we can expect $\langle 1/d \rangle^{-1}/\langle d \rangle = (m + 4)(m + 2)/(m + 1)^2 \sim 1.4$ for $m = 10$, which amounts to 90% of the observed ratio of 1.5. The second source may be that the sample also has the distribution in the axial ratio p. Indeed, on the electron micrographs of brush border membrane vesicles (Hopfer et al., 1983), are found some ellipsoidal shapes with axial ratios down to 0.2 (or up to 5; it is not clear on the micrographs whether the vesicles are prolate or oblate). In the above analysis of the static scattering intensity, we ignored the distribution in p. Thus, $m \sim 15$ for $p = 0.5$ may be the upper bound of the m value. Although not yet been fully examined, our samples used in the accompanying paper (Miyamoto et al., 1988) could be characterized to be the suspensions of ellipsoidal vesicles with $p \sim 0.5$ and $m \sim 10$.

The osmotic swelling experiment can be possible for such ellipsoidal vesicles, if they expand keeping the axial ratio and its distribution unchanged. In such a situation, however, the size of the membrane modulus M is never absolute, because the diameter d evaluated from $\langle \bar{\Gamma}/K^2 \rangle$ and not from $\langle D \rangle$ by use of Eq. 5 is not correct in the absolute size. If we put $d = (1 + \Delta)d^o$, Eq. 1 gives $M = (1 + \Delta)M^o$, where the superscript 'o' denotes the true quantity. This Δ may depend not only on the size and shape distributions of the vesicles but also on the scattering angle. Nevertheless, the relative size of the change in the M-value depending on different conditions (such as activation of a transport system of the membrane given in the accompanying paper) is very meaningful, because Δ is highly constant for a given preparation at a fixed scattering angle. It should be emphasized again that the scattering angle at the measurement is carefully determined to avoid the region where $\bar{\Gamma}/K^2$ changes strongly with K^2.

CONCLUSIONS

The considerations given above clarified some complications in determining the size of swelling by dynamic light scattering. These complications mostly come from the

"shell" structure of the scatterers with submicron sizes; namely, from the notch filtering action of the modified scattering function.

For spherical vesicles, the average value of the diameter d estimated from $\langle D \rangle$, and hence the size of elastic modulus M, depend on the $d_n K$ value. When a correlation between M and d_n is discussed, a characteristic feature of the dependence on K^2 of $\langle D \rangle$ as shown in Fig. 2 *a* should carefully be examined. Otherwise, substantial over/under-estimation of M would happen to occur.

For ellipsoidal vesicles, the contribution to the apparent diffusion coefficient ($\bar{\Gamma}/K^2$) from the rotational motion of ellipsoids produces another complication. In addition, Eq. 1 has been derived for a spherical shell. However, the estimated size of M is still a good measure of the membrane elastic modulus.

At the moment, however, the present method is probably the most rapid, accurate, and powerful in the study of elastic properties of membrane vesicles with submicron sizes under various conditions.

S. Miyamoto thanks the postdoctoral fellowship from Mitsubishi-Kasei Institute of Life Sciences.

Received for publication 29 June 1987 and in final form 30 November 1987.

REFERENCES

Aragon, S. R., and R. Pecora. 1976. Theory of dynamic light scattering from polydisperse systems. *J. Chem. Phys.* 64:2395–2404.

Berne, B., and R. Pecora. 1975. Dynamic Light Scattering. John Wiley & Sons Inc., New York. 376 pp.

Chu, B. 1974. Laser Light Scattering. Academic Press, Inc., New York. 317 pp.

Fujime, S., and K. Kubota. 1985. Dynamic light scattering from dilute suspensions of thin discs and thin rods as limiting forms of cylinder, ellipsoid and ellipsoidal shell of revolution. *Biophys. Chem.* 23:1–13.

Hopfer, U., T. D. Crowe, and B. Tandler. 1983. Purification of brush border membrane by thiocyanate treatment. *Anal. Biochem.* 131:447–452.

Koppel, D. E. 1972. Analysis of macromolecular polydispersity in intensity correlation spectroscopy: the method of cumulant. *J. Chem. Phys.* 57:4814–4820.

Li, W., T. S. Aurora, T. H. Haines, and H. Z. Cummins. 1986. Elasticity of synthetic phospholipid vesicles and submitochondrial particles during osmotic swelling. *Biochemistry.* 25:8220–8229.

Maeda, T., and S. Fujime. 1984. Spectrum of light quasielastically scattered from solutions of very long rods in dilute and semidilute regimes. *Macromolecules.* 17:1157–1167.

Miyamoto, S., T. Maeda, and S. Fujime. 1988. Change in membrane elastic modulus on activation of glucose transport system of brush border membrane vesicles studied by osmotic swelling and dynamic light scattering. *Biophys. J.* 53:505–512.

Moriguchi, S., K. Udagawa, and S. Hitotsumatsu. 1959. Mathematical Formulas I (in Japanese). Iwanami, Tokyo. p 231.

Norisuye, T., and H. Yu. 1977. Osmotically-induced and photo-induced deformations of disk membranes. *Biochim. Biophys. Acta.* 471:436–452.

Perrin, F. 1934. Mouvement Brownien d'un ellipsoide (I): dispersion dielectrique pour des molecules ellipsoidales. *J. Phys. Radium.* 7:497–511.

Sun, S.-T., A. Milon, T. Tanaka, G. Ourisson, and Y. Nakatani. 1986. Osmotic swelling of unilamellar vesicles by the stopped flow light scattering method: elastic properties of vesicles. *Biochim. Biophys. Acta.* 860:525–530.

Yu, H. 1983. Structure and dynamics of disk membrane vesicles. *In* The Application of Laser Light Scattering to the Study of Biological Motion. J. C. Earnshaw and M. W. Steer, editors. Plenum Publishing Corp., New York. 367–382.